




**${}^{6,7}\text{Li} + {}^{27}\text{Al}$  reactions close to and below the Coulomb barrier**J. Kührtreiber, P. Hille, O. Forstner <sup>\*</sup>, H. Friedmann <sup>†</sup>, A. Pavlik , and A. Priller  
*University of Vienna, Faculty of Physics, 1090 Wien, Austria*

(Received 30 March 2020; revised 11 February 2021; accepted 6 May 2021; published 9 June 2021)

The reactions  ${}^{6,7}\text{Li} + {}^{27}\text{Al}$  were compared with the reactions  ${}^{17,18}\text{O} + {}^{16}\text{O}$  which form the same compound nuclei  ${}^{33,34}\text{S}$ . Cross-section data for the reactions  ${}^{6,7}\text{Li} + {}^{27}\text{Al}$  were derived from experimentally determined  $\gamma$ -ray production cross sections for transitions in several residual nuclei. For the reactions  ${}^{17,18}\text{O} + {}^{16}\text{O}$  experimental results from the literature were used. It could be shown that the weakly bound projectiles  ${}^{6,7}\text{Li}$  undergo not only fusion processes, but also breakup reactions quite in contrast to the tightly bound projectiles  ${}^{18}\text{O}$  and  ${}^{17}\text{O}$ , respectively. Especially below the Coulomb barrier such direct reactions play an important role in competition to complete fusion. Calculations based on the statistical model agree well with the available data for  ${}^{17,18}\text{O} + {}^{16}\text{O}$ , but failed to represent the behavior of the experimentally determined production cross sections for the evaporation residues in the reactions  ${}^{6,7}\text{Li} + {}^{27}\text{Al}$ . But coupled-channel codes and calculations based on a nucleus-nucleus proximity potential are able to reproduce the energy dependence of the complete fusion cross sections.

DOI: [10.1103/PhysRevC.103.064605](https://doi.org/10.1103/PhysRevC.103.064605)**I. INTRODUCTION**

Radioactive beams have opened the way to regions in the nuclide chart which could not be reached by other methods (see, e.g., Geissel *et al.* [1]). Since radioactive projectiles are often weakly bound, breakup before complete fusion is a matter of interest. Additionally, nuclear reactions close to and below the Coulomb barrier (CB) are of eminent importance during the formation of the elements by astrophysical processes. In many cases the cross sections are too small to be experimentally determined. Therefore, it is necessary to understand the mechanism of these nuclear reactions to estimate the excitation functions by model calculations. It is not yet clear if for weakly bound projectiles a breakup or a partial fusion contribute substantially to nuclear reaction close and below the CB. Tripathi *et al.* [2] as well as the measurements of Dasgupta *et al.* [3] ( ${}^7\text{Li} + {}^{209}\text{Bi}$ ), Figueira *et al.* [4] ( ${}^{6,7}\text{Li} + {}^{144}\text{Sm}$ ), and Rath *et al.* [5] ( ${}^6\text{Li} + {}^{144}\text{Sm}$ ) support these ideas. A relative large number of experiments deal with the question of complete fusion (CF) suppression close to and below the CB concerning reactions of light particles with different types of target material. Here only a few of these publications are mentioned. Hinde *et al.* [6] also observed a fusion suppression but depending on the atomic number of the target. Interestingly some authors, such as Parkar *et al.* [7] ( ${}^7\text{Li} + {}^{12}\text{C}$ ), Mukherjee and co-workers [8] ( ${}^{6,7}\text{Li} + {}^{16}\text{O}$ ), [9] ( ${}^6\text{Li} + {}^{12,13}\text{C}$ ), [10] ( ${}^{12}\text{C} + {}^7\text{Li}$ ), and Ray *et al.* [11] ( ${}^{6,7}\text{Li} + {}^{24}\text{Mg}$ ) did not see any fusion suppression. These different behaviors may be explained by a decreasing

breakup effect with a decreasing atomic number of the target as observed by Hinde *et al.* [6] and Pakou *et al.* [12]. De Barbará *et al.* [13] did not observe fusion suppression in the  ${}^9\text{Be} + {}^{27}\text{Al}$  system and for  ${}^6\text{Li} + {}^{27}\text{Al}$ . For  ${}^7\text{Li} + {}^{27}\text{Al}$  de Barbará *et al.* state a possible fusion suppression but do not draw final conclusions due to problems with the analysis of this data set. Gasques *et al.* [14] found a systematic suppression of weakly bound nuclei  ${}^{6,7}\text{Li}$ ,  ${}^9\text{Be}$ , and  ${}^{10,11}\text{B}$  on targets of  ${}^{208}\text{Pb}$  and  ${}^{209}\text{Bi}$  as a function of breakup threshold energy.

However, most often significant fusion enhancement close or below the CB could be observed by neutron-rich projectiles [15–17]. Microscopic calculations are unable to explain this behavior. More insight into the reaction process may be deduced from an isotopic chain of weakly bound nuclei with increasing neutron number (e.g., Refs. [18,19] and similar work). The reactions  ${}^7\text{Li} + {}^{27}\text{Al}$  and  ${}^6\text{Li} + {}^{27}\text{Al}$  are of special interest to improve the database for such projectiles: These data should give better insight whether the fusion process is preceded or competed by a breakup process (see Canto *et al.* [20]). To study these reactions experimentally,  ${}^{6,7}\text{Li}$  ions were accelerated to laboratory energies between 6 and 13 MeV and the formed reaction products in an  ${}^{27}\text{Al}$  foil were measured by  $\gamma$ -ray spectrometry. The excitation functions for the formation of the most important nuclear reaction products were determined and compared with the results of investigations on the reaction of the tightly bound nuclei  ${}^{17,18}\text{O} + {}^{16}\text{O}$  (Thomas *et al.* [21]) leading to the same compound nuclei  ${}^{33,34}\text{S}$ . Since in this case both reaction partners are magic nuclei it can be expected that breakup is of minor importance and CF is the dominant process. For a meaningful comparison it is necessary to choose beam energies in order to get overlapping excitation energies for the compound nuclei produced in both reactions. Obviously, the spin and parity distributions in the highly excited compound nuclei will not be identical.

<sup>\*</sup>Present address: University Jena, Institut für Optik und Quantenelektronik, 07743 Jena, Germany.

<sup>†</sup>Corresponding author: [harry.friedmann@univie.ac.at](mailto:harry.friedmann@univie.ac.at)

Statistical model calculations using the EMPIRE code [22] were used to get a quantitative control over this effect and to estimate the remaining contributions of direct reaction processes. EMPIRE is a computer code bundle based on several statistical model (Hauser-Feshbach) reaction codes.

In the case of the formation of a compound nucleus this nucleus is in a highly excited state and particles, such as  $n$ ,  $\alpha$ ,  $p$ ,  $d$ , and  $t$ , can be evaporated until the excitation energy of the evaporation residue is below the binding energy of these particles to the remaining nucleus. Then, the energy can only be reduced by  $\gamma$  and/or  $\beta$  emission. In these experiments the excitation functions for the formation of the different reaction products (RP) were determined by  $\gamma$  spectrometry and compared with calculations based on the statistical model. It is not necessary to measure absolute production cross sections to observe additional contributions of breakup or transfer reactions. The ratio in the production rate of the different RPs should be independent from the formation of the compound nucleus in the case of equal excitation energy, spin, and parity distribution. Any deviation from the ratios measured in the  $^{17,18}\text{O} + ^{16}\text{O}$  reactions (Thomas *et al.* [21]) which can be assumed as CF reactions, should allow to identify additional contributions by breakup and transfer reactions.

## II. EXPERIMENTAL SETUP

The accelerator VERA [23] at the University of Vienna was used to bombard Al-foils ( $0.542 \pm 0.006 \text{ mg/cm}^2$ ) with  $^6,7\text{Li}$  with energies between 6 and 13 MeV. Negative LiF ions were formed in a sputter ion source, energy separated in an electrostatic unit and mass separated in a  $90^\circ$  magnet. Then, the beam was transferred into a tandem accelerator where at the high voltage terminal the LiF molecules were destroyed within a gas stripper pipe, and positive  $\text{Li}^{2+}$  and  $\text{Li}^{3+}$  ions could be selected by an analyzing magnet. After that, the beam was focused on the Al foil (Goodfellow, purity 99.9%, thickness  $2 \mu\text{m}$  with an uncertainty of below 5%, determined by measurements of several samples of the same foil) which was electrically coupled to a Ta plate behind it which formed the charge collector of a Faraday cup (FC). With this setup the current caused by the Li ions hitting the foil could be measured directly. In front of this Faraday cup another Faraday cup was installed with a wider opening for the beam entrance and a central hole in the collector plate. This additional cup was used to survey and adjust the beam to be focused to the Al foil inside the second cup. Both cups were run with a counter electrode on  $-100 \text{ V}$  to suppress secondary electrons from the collector plates. A HPGe detector (ORTEC<sup>®</sup> GAMMA-X, 25% relative efficiency) was mounted outside the vacuum system as close as possible to the Al foil (Figs. 1 and 2). Depending on particle charge and particle energy the measured beam currents were in the range between 0.5 and 100 nA.

The qualitative and quantitative identification of the reaction products were performed by  $\gamma$ -ray spectrometry. The signals from the HPGe detector were amplified by an ORTEC<sup>®</sup> 571 spectroscopy amplifier and then fed into a 16k channels Canberra 8713 ADC. The stability of the electronic circuit was monitored by using an ORTEC<sup>®</sup> 419 precision

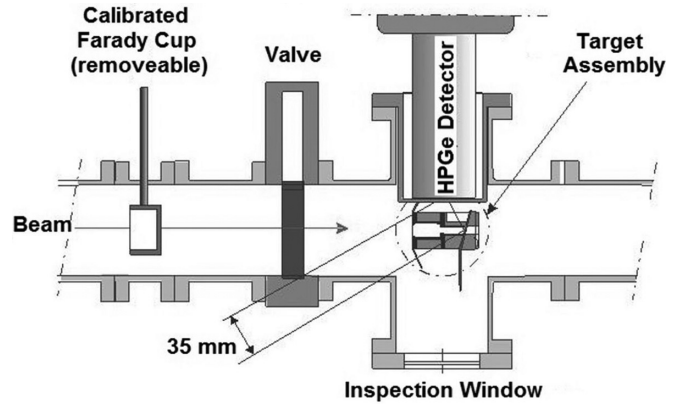


FIG. 1. Overview of the experimental setup in the target area.

pulse generator. The digitized pulse height signals from the  $\gamma$  detector were collected in list mode which means each  $\gamma$  event was stored together with the time signal from a real-time clock (FAST ComTec MPA-3). This offers the possibility to sort the events in energy bins as well as in time bins. The latter allows distinguishing between prompt  $\gamma$ -ray emission and  $\gamma$  rays from the decay of radioactive reaction products. It was possible to identify several reaction products by their characteristic  $\gamma$ -emission energy and observing their decay in time. The detector efficiency was determined by several calibration sources which were placed at the target position before and after the experiment. Background spectra were taken with the beam off and with beam on but without the target mounted. The beam energy was calibrated according to Forstner *et al.* [24]. The beam energy decay in the target foil and the mean projectile energy were calculated by the computer code SRIM [25]. Table I gives an overview for the used energies.

The experiment started by focusing the beam onto the second Faraday cup within the target assembly but without the Al foil. This Faraday cup and, therefore, the particle flux was calibrated by repeated measurements using a calibrated Faraday cup in front of the target after the beam has become stable. Then the valve was closed, and the target foil was inserted via the inspection window flange. After evacuating

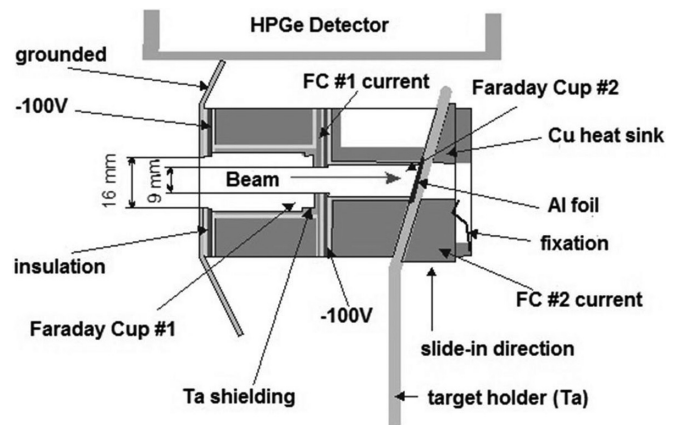


FIG. 2. Target assembly.

TABLE I. Beam energy, mean energy in the target foil calculated using the SRIM [25] code, and mean center-of-mass energy in the target and excitation energy of the compound nucleus. All energies are given in MeV. The mean energy in the target for  ${}^6\text{Li}$  and  ${}^7\text{Li}$  do not differ within the uncertainty of the calculation which is estimated to about 5%. The uncertainty of the accelerator voltage is below 2 kV, thus, the uncertainties in the beam energy is in all cases below 10 keV.

Beam energy (MeV)	Mean Energy in the Target (MeV)	Center of mass energy (MeV) for the Projectile		Compound Nucleus Excitation Energy (MeV) for Projectile	
		${}^6\text{Li}$	${}^7\text{Li}$	${}^6\text{Li}$	${}^7\text{Li}$
6.0	5.6	4.4	4.4	27.9	32.1
7.0	6.6	5.2	5.2	28.7	32.9
8.0	7.6	6.1	6.1	29.6	33.7
9.0	8.6	6.9	6.9	30.4	34.5
10.0	9.7	7.7	7.7	31.2	35.3
11.0	10.7	8.5	8.5	32.0	36.1
12.0	11.7	9.3	9.3	32.8	36.8
13.0	12.7	10.1	10.1	33.6	37.6

the target assembly and starting the data acquisition, the valve was opened, the calibrated Faraday cup was removed, and the beam hit the target. The currents in Faraday cups no. 1 and no. 2 were recorded in intervals of 5 s. FC no. 1 did not show any measurable current which demonstrated that the whole beam cross section hits the target. After 20 min of irradiation the calibrated Faraday cup was brought into the beam to stop the irradiation of the target, but the data acquisition continued for further 10 to 20 min to observe the decay of the reaction products.

Figure 3 shows a  $\gamma$ -ray spectrum acquired during the irradiation time whereas in Fig. 4 the count rate of 1779-keV transition in the radioactive decay of  ${}^{28}\text{Al}$  as a function of time can be seen.

Additionally, coincidence effects have to be regarded when deriving absolute cross-section values from the measured data. Because the detector is placed close to the target the probability for summing effects cannot be neglected.  $\gamma$  coincidences can either increase the full-energy peak by some (two) observed transitions with a summing energy which is by chance equal to the observed full-energy peak or reduce the area when a coincident transition comes along with the

full-energy emission. To correct for the latter effect the branching ratios of the  $\gamma$  transitions and the feeding of the different levels of the RP must be known. Here, the branching ratios were taken from the NUDAT database [26], the feeding of the levels was calculated using the EMPIRE code [22]. The corrections for these summing effects were made using the peak to total ratios as described by Watanabe *et al.* [27].

### III. ANALYSIS

Aim of the analysis of our experimental data was to derive cross-section ratios of the production cross sections of various reaction products to the CF cross sections for  ${}^7\text{Li} + {}^{27}\text{Al}$  and  ${}^6\text{Li} + {}^{27}\text{Al}$ , respectively. Comparing these ratios with the corresponding values for  ${}^{17,18}\text{O} + {}^{16}\text{O}$  derived from the results of Thomas *et al.* [21] permits drawing conclusions on reaction mechanisms different from complete fusion followed by evaporation. Thomas *et al.* calculated  $\sigma(\text{CF})$  by summing up all partial cross sections. As the complete fusion cross section cannot be determined from our experimental results, we used the following approach to estimate the above mentioned cross-section ratios. It can be assumed that in the case of the  ${}^7\text{Li} + {}^{27}\text{Al}$   ${}^{32}\text{P}$  is only produced by evaporation from the compound nucleus  ${}^{34}\text{S}$ . The same assumption is valid for  ${}^{31}\text{P}$  and  ${}^{33}\text{S}$  for the  ${}^6\text{Li}$ -induced reaction. Therefore, the ratio of the cross section for the formation of  ${}^{32}\text{P}$  from the compound nucleus  ${}^{34}\text{S}$  and the cross section of the CF,  $\sigma({}^{32}\text{P})/\sigma(\text{CF})$ , was taken from the reaction  ${}^{18}\text{O} + {}^{16}\text{O}$  [21]. Then  $\sigma(\text{CF})$  for the reaction  ${}^7\text{Li} + {}^{27}\text{Al}$  could be calculated by using the measured cross-section  $\sigma({}^{32}\text{P})$  from this experiment. In the same way the ratio  $\sigma({}^{31}\text{P})/\sigma(\text{CF})$  was derived using the results of Ref. [21] for the reaction  ${}^{17}\text{O} + {}^{16}\text{O}$ . Calculations using the codes EMPIRE [22] and CCFULL [28] showed that the different formation of the compound nucleus, causing different spin and parity distributions, gave only insignificant difference in the results in the evaporation process according to EMPIRE. Thus, the cross-section ratios for the RP are not significantly altered (worst case approximately 40% at 32 MeV for  ${}^{29}\text{Si}$ ). Results of these calculations for the  ${}^7\text{Li} + {}^{27}\text{Al}$  reaction can

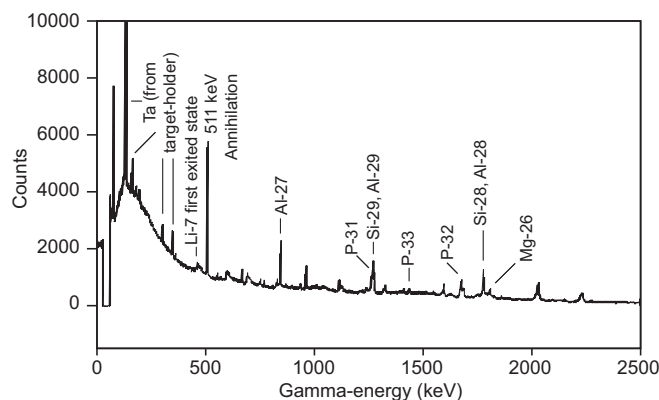


FIG. 3. Prompt  $\gamma$  spectrum from the reaction  ${}^7\text{Li} + {}^{27}\text{Al}$  at 13 MeV. Indicated are the peaks which could be used for the calculations.

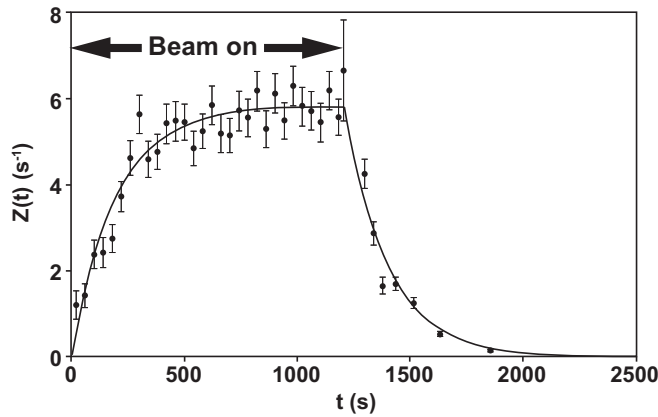


FIG. 4. Count rate of the 1779-keV transition in the radioactive decay of  $^{28}\text{Al}$ . The ion beam was turned on at  $t = 0$  and kept constant for 1200 s, then, it was turned off, and the typical decay of the reaction product could be observed. The solid line fits the buildup and the decay of  $^{28}\text{Al}$  using the known decay constant [26].

be seen in Fig. 5. The accordance for the  $^6\text{Li} + ^{27}\text{Al}$  reaction with the  $^{17}\text{O} + ^{16}\text{O}$  data is quite similar.

Figure 6 shows the cross section for complete fusion, derived from the ratio  $\sigma(\text{CF})/\sigma(^{31,32}\text{P})$  from Thomas *et al.* [21] multiplied by the results of the measured  $\sigma(^{31,32}\text{P})$  from our experiments. In addition, data from Kalita *et al.* [29] can also be seen in that figure, which cover projectile energies above 10 MeV. The cross-sections  $\sigma(^{31}\text{P})$  and  $\sigma(^{32}\text{P})$  were computed from the prompt 1266-keV transition in  $^{31}\text{P}$  and from the 1677-keV transition in  $^{32}\text{P}$ . The cross sections could not be derived for all beam energies listed in Table I.

### A. The $^7\text{Li} + ^{27}\text{Al}$ reaction

Besides the formation of  $^{34}\text{S}$  by complete fusion the projectile  $^7\text{Li}$  can undergo a breakup into an  $\alpha$  particle and a triton  $t$ . Thus, the reaction channels  $\alpha + ^{27}\text{Al}$  and  $t + ^{27}\text{Al}$  have to be

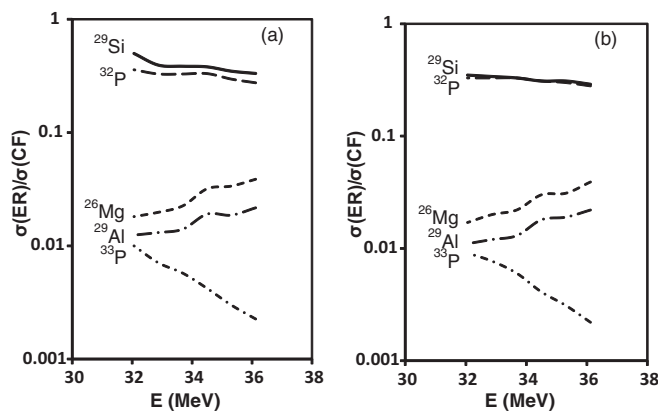


FIG. 5. EMPIRE [22] results for cross-section ratios for the formation of the evaporation residue and the CF concerning the compound nucleus  $^{34}\text{S}$  formed by the reaction  $^7\text{Li} + ^{27}\text{Al}$  (a) and  $^{18}\text{O} + ^{16}\text{O}$  (b) at the same excitation energy. Shown are RPs which are measured in this experiment.

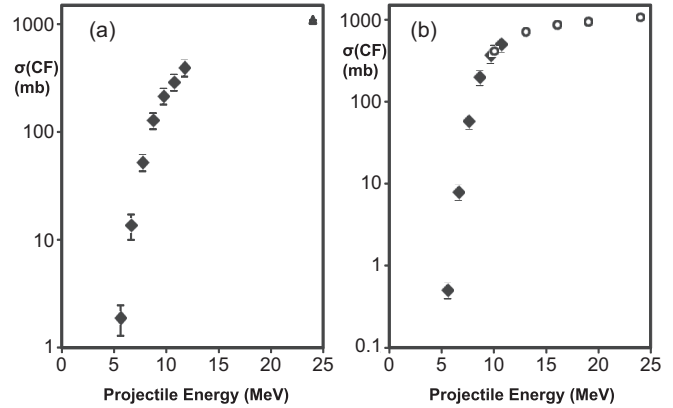


FIG. 6. Complete fusion cross section in millibarns as a function of the projectile energy for the reactions (a)  $^6\text{Li} + ^{27}\text{Al}$ ; (b)  $^7\text{Li} + ^{27}\text{Al}$ . The CB is at 8.1 MeV (derived from a proximity potential). The diamonds are data derived from our experiments; the open circles are data from Kalita *et al.* [29], and the triangle indicates the lowest data point from Padron *et al.* [30].

observed too. Furthermore, the transfer reactions  $n + ^{27}\text{Al}$  and  $p + ^{27}\text{Al}$  are also possible. Therefore, a number of reaction products can be expected, depending on the  $Q$  value of the reactions, the height of the CB and the center-of-mass energy in the experiment.

From the prompt  $\gamma$  spectra the RP  $^{33}\text{P}$ ,  $^{32}\text{P}$ ,  $^{29}\text{Si}$ , and  $^{26}\text{Mg}$  and from the  $\gamma$  spectra after the end of the irradiation and their decay the nuclides  $^{29}\text{Al}$ ,  $^{28}\text{Al}$ , and  $^{30}\text{P}$  (511 keV annihilation peak) could be identified, and their relative production cross sections could be measured.

In most cases the branching ratios of the  $\gamma$  transitions in the RP play a significant role in the determination of the absolute cross sections. To compare the reaction  $^7\text{Li} + ^{27}\text{Al}$  with the reaction  $^{18}\text{O} + ^{16}\text{O}$  the same branching ratios as used by Ref. [21] were taken for this experiment too.

Ratios  $[\sigma(\text{RP})/\sigma(\text{CF})]$  were derived from the measured  $\gamma$ -ray production cross sections and compared with the data of the  $^{18}\text{O} + ^{16}\text{O}$  reaction to check for contribution of reaction mechanism other than complete fusion.

In a first step the ratio  $\sigma(^{32}\text{P})/\sigma(\text{CF})$  as determined by Thomas *et al.* [21] was compared with calculations by the EMPIRE [22] code (Fig. 7). Although in the range below 35 MeV compound nucleus excitation energy ( $E_{\text{CN}}$ ) the measured data are consistent with the calculations within the estimated uncertainties, the measured data at higher excitation energies are well below the calculated values. The reason may be either a suppression of the  $^{32}\text{P}$  channel which could not be realized by the calculation or the fact that  $\sigma(\text{CF})$ , which could not be measured directly, was overestimated by Thomas *et al.* [21]. A possible reason for the latter may be the significantly higher contribution of  $^{26}\text{Mg}$  at higher energies  $[\sigma(^{26}\text{Mg})/\sigma(\text{CF})]$  up to a factor of 5 larger, see Fig. 9] in the published data compared with EMPIRE calculations.

Nevertheless, the derived  $\sigma(\text{CF})$  values from the  $\sigma(^{32}\text{P})/\sigma(\text{CF})$  ratios from Ref. [21] and the measured data fit very well with the results of a calculation using the coupled channel code CCFULL [28] as can be seen from Fig. 8.

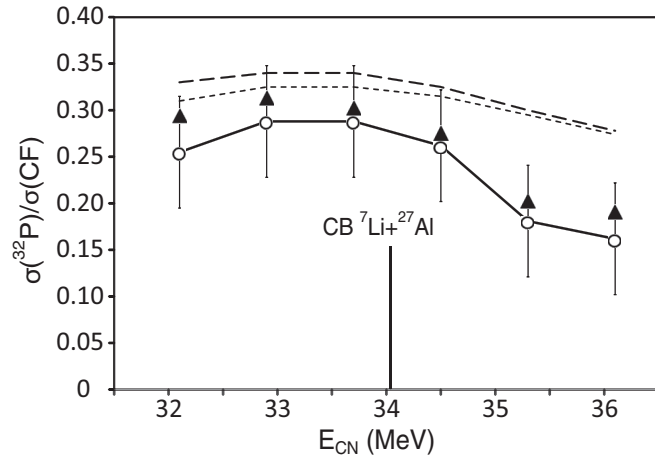


FIG. 7. Cross-section ratios  $\sigma({}^{32}\text{P})/\sigma(\text{CF})$  from Ref. [21] (open circles) with estimated uncertainties. The triangles indicate a correction to the data by using calculated  $\sigma({}^{26}\text{Mg})/\sigma(\text{CF})$  values. The upper dashed line is the result of an EMPIRE [22] calculation for the  ${}^{18}\text{O} + {}^{16}\text{O}$  reaction, and the lower dashed line is the result of the calculation for the  ${}^7\text{Li} + {}^{27}\text{Al}$  reaction.

This result could even be achieved without using rotational and vibrational coupling (inert target). It should be mentioned that CCFULL was specially developed to model fusion of relatively light ions close to the Coulomb barrier.

The determination of the RP  ${}^{33}\text{P}$  by measuring the 1432-keV  $\gamma$  transition could only be performed with a relatively large uncertainty (approximately  $\pm 50\%$ ). Below the CB the results agree very well with the results from the reaction  ${}^{18}\text{O} + {}^{16}\text{O}$ , whereas above the CB the ratio  $\sigma({}^{33}\text{P})/\sigma(\text{CF})$  is systematically about 30% higher than from Ref. [21]. Generally, the experimental results are about a factor of 3 higher than the results from calculations using the EMPIRE code [22].

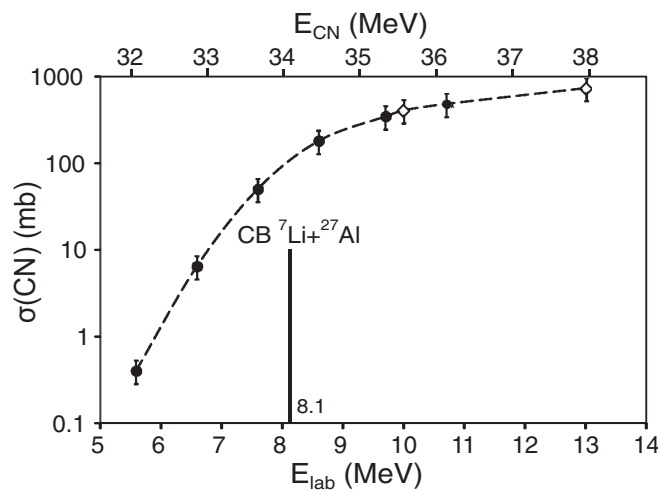


FIG. 8. Complete fusion excitation function for the reaction  ${}^7\text{Li} + {}^{27}\text{Al}$ . The full circles are the results from our CCFULL [28] calculations using the  $\sigma({}^{32}\text{P})/\sigma(\text{CF})$  ratio from the reaction  ${}^{18}\text{O} + {}^{16}\text{O}$  as published in Ref. [21]. The open diamond represents a datum from Kalita *et al.* [29]. The CB was calculated from a proximity potential.

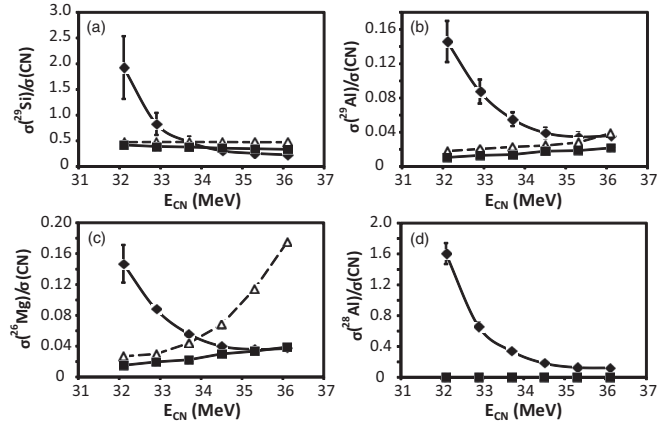


FIG. 9. Ratio of the formation cross section for different reaction products versus the complete fusion cross section: Experimental and calculated (compound nucleus) data for the reaction  ${}^7\text{Li} + {}^{27}\text{Al}$  and  ${}^{18}\text{O} + {}^{16}\text{O}$ . The solid lines with the full diamonds are the results from this experiment, the dashed lines with the open triangles are the results from the  ${}^{18}\text{O} + {}^{16}\text{O}$  experiment [21], and the solid lines with the full squares are the results from EMPIRE [22] calculations. The experimental observed increase at low energies for the reaction  ${}^7\text{Li} + {}^{27}\text{Al}$  is an indication for additional other reaction mechanisms than the pure compound reaction.

The formation of  ${}^{29}\text{Si}$  was detected via the 1273-keV line. The peak areas were corrected for a contribution from the decay of  ${}^{29}\text{Al}$ .  ${}^{29}\text{Si}$  can be formed by a breakup of the projectile via the reactions  ${}^{27}\text{Al}(t, n){}^{29}\text{Si}$  or  ${}^{27}\text{Al} + d \rightarrow {}^{29}\text{Si}$  too. Comparing the results for the reactions  ${}^{18}\text{O} + {}^{16}\text{O}$  and  ${}^7\text{Li} + {}^{27}\text{Al}$  the ratios of  $\sigma({}^{29}\text{Si})/\sigma(\text{CF})$  show a significant difference: At energies above the CB both experiments give approximately the same values which fit also to the results of the EMPIRE calculations. However, below the CB the results from this experiment increase substantially with decreasing energy. This gives a strong indication for an additional

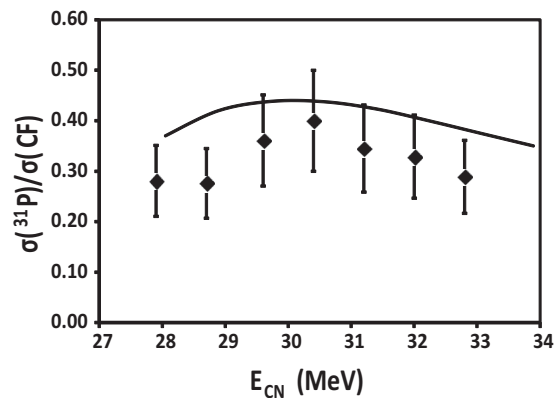


FIG. 10. Ratio of the formation cross section for  ${}^{31}\text{P}$  versus the complete fusion cross section: Full diamonds with uncertainty bars are from the  ${}^{17}\text{O} + {}^{16}\text{O}$  experiments [21] (uncertainty on the order of 25% derived from the diagrams in Ref. [21]), and the solid line represents compound nucleus calculations for the reaction  ${}^6\text{Li} + {}^{27}\text{Al}$  (EMPIRE code [22]) data. EMPIRE gives nearly the same results for  ${}^{17}\text{O} + {}^{16}\text{O}$ .

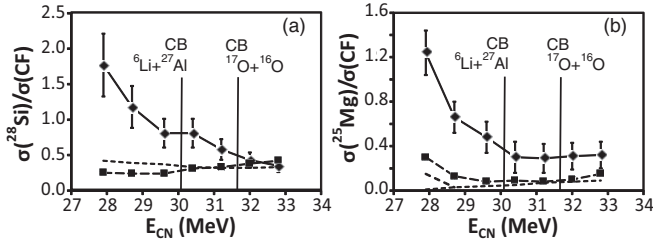


FIG. 11. Ratio of the formation cross section for (a)  $^{28}\text{Si}$  and (b)  $^{25}\text{Mg}$  versus the complete fusion cross section for  $^{17}\text{O} + ^{16}\text{O}$  (full squares, dashed line) and  $^6\text{Li} + ^{27}\text{Al}$  (full diamonds, solid line). In the figure the results of the compound nucleus calculations (EMPIRE [22], short dashed line) cannot be differentiated between the two formation processes. Only for  $^{25}\text{Mg}$  at the lowest energy of the compound nucleus a small difference in the ratio can be seen (higher values for the  $^6\text{Li} + ^{27}\text{Al}$  reaction).

contribution of a break up reaction  $^{27}\text{Al}(t, n)^{29}\text{Si}$  and/or a transfer reaction  $^{27}\text{Al} + d \rightarrow ^{29}\text{Si}$  [Fig. 9(a)]. Other types of reactions are energetically not possible.

Similar effects could be observed for the ratios  $\sigma(^{29}\text{Al})/\sigma(\text{CF})$  [Fig. 9(b)],  $\sigma(^{26}\text{Mg})/\sigma(\text{CF})$  [Fig. 9(c)] and  $\sigma(^{28}\text{Al})/\sigma(\text{CF})$  [Fig. 9(d)].

The strong increase in  $\sigma(\text{RP})/\sigma(\text{CF})$  could not be reproduced by the EMPIRE codes. Therefore, other calculation models were tested. The CCFULL code [28] with only ground-state levels as well as calculations based on a nucleus-nucleus proximity potential [31–33] give sufficient results for  $\sigma(\text{CF})$  derived from the measured  $\sigma(^{32}\text{P})$  and the ratio  $\sigma(^{32}\text{P})/\sigma(\text{CF})$  from Ref. [21]. All these computer codes need a couple of parameters to fit the measured data, however, the shape of the excitation function for  $\sigma(\text{CF})$  could only be reproduced by the coupled-channel code and the proximity potential calculation.

The EMPIRE code was used to estimate the evaporation residue production rates via a compound nucleus reaction. The code is a combination of different codes treating different problems during the calculation of the cross sections based on the statistical model of nuclear reactions. Instead of using the integrated code part for calculating  $\sigma(\text{CF})$ , the code CCFULL was used because the results were in better agreement with the experimental results.

The uncertainty budget is different for the different RP and consists of the contribution by the target (density and thickness) and in combination with the calculated energy loss by the computer code SRIM [25] (generally on the order of 5%),

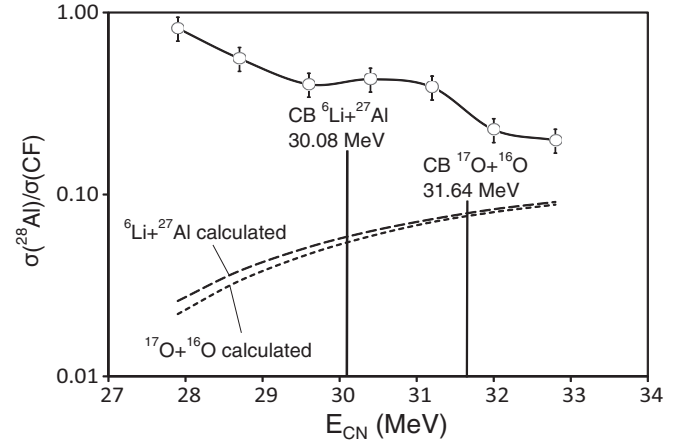


FIG. 12. Ratio of the formation cross section for  $^{28}\text{Al}$  versus the complete fusion cross section. The solid lines with the open circles are the experimental data from this experiment; dotted lines are compound nucleus calculations (EMPIRE [22]).

the uncertainty in the determination of the particle flux by measuring the current from the Faraday cup (below 1%), the detector efficiency, determined by calibration sources ( $^{152}\text{Eu}$ ,  $^{60}\text{Co}$ ), the determination of the peak areas and the summing corrections including the random uncertainty from the counting statistics (on the order of 10% and below for most RP), the branching ratios which were taken from Ref. [21] (digitized from the printed publication) for the ratios  $\sigma(\text{RP})/\sigma(\text{CF})$  and from NUDAT [26] for the absolute cross sections and finally the  $\sigma(\text{CF})$  values, also taken from Ref. [21] with the estimated uncertainties given in Ref. [34].

The on-line reaction code from the “Nuclear Reactions Video Project (NRV)” [34] was used especially to check the results of the calculations described above for plausibility. This was important because the used codes need a number of parameters for input to fit the results to the observed data.

### B. The $^6\text{Li} + ^{27}\text{Al}$ reaction

Again, besides the formation of the compound nucleus  $^{33}\text{S}$  by complete fusion a number of reaction products can be expected caused by breakup of  $^6\text{Li}$ , depending on the  $Q$  value of the reactions, the height of the CB, and the center-of-mass energy in the experiment.

From the prompt  $\gamma$  spectra the following RP could be identified and measured:  $^{31}\text{P}$ ,  $^{28}\text{Si}$ , and  $^{25}\text{Mg}$ . From the  $\gamma$

TABLE II. Resultant cross section for the RP in millibarns with its  $1\sigma$  uncertainty for the reaction  $^7\text{Li} + ^{27}\text{Al}$  as a function of the excitation energy of the compound nucleus  $^{34}\text{S}$  in MeV using  $\sigma(\text{CF})$  from Ref. [21].

$E_{\text{CN}}$ (MeV)	$^{33}\text{P}$	$^{32}\text{P}$	$^{30}\text{P}$	$^{29}\text{Si}$	$^{29}\text{Al}$ delayed	$^{28}\text{Al}$ delayed	$^{26}\text{Mg}$	CF
32.1	$0.06 \pm 0.01$	$0.13 \pm 0.02$	$0.04 \pm 0.03$	$0.79 \pm 0.25$	$0.06 \pm 0.01$	$0.96 \pm 0.08$	$0.07 \pm 0.01$	$0.41 \pm 0.07$
32.9	$0.26 \pm 0.01$	$2.14 \pm 0.28$	$0.15 \pm 0.10$	$5.4 \pm 1.4$	$0.57 \pm 0.09$	$6.0 \pm 0.5$	$0.30 \pm 0.03$	$6.5 \pm 0.9$
33.7	$0.87 \pm 0.03$	$15.8 \pm 1.8$	$0.28 \pm 0.15$	$24 \pm 5$	$2.8 \pm 0.4$	$21 \pm 2$	$1.0 \pm 0.1$	$50 \pm 6$
34.5	$2.29 \pm 0.07$	$51 \pm 6$	$0.7 \pm 0.4$	$55 \pm 12$	$7.0 \pm 1.0$	$35 \pm 3$	$2.2 \pm 0.2$	$178 \pm 20$
35.3	$4.1 \pm 0.13$	$70 \pm 8$	$1.5 \pm 1.2$	$88 \pm 19$	$11.8 \pm 1.7$	$45 \pm 4$	$3.4 \pm 0.4$	$340 \pm 39$
36.1	$4.6 \pm 0.14$	$92 \pm 11$	$2.0 \pm 0.8$	$109 \pm 23$	$17 \pm 3$	$61 \pm 5$	$3.9 \pm 0.4$	$473 \pm 54$
36.8	$6.1 \pm 0.2$	$96 \pm 11$	$3.3 \pm 2.9$		$20 \pm 3$	$63 \pm 6$	$5.5 \pm 0.6$	
37.6	$7.3 \pm 0.2$	$119 \pm 13$	$4.7 \pm 2.3$		$26 \pm 4$	$76 \pm 6$	$5.9 \pm 0.7$	

TABLE III. Resultant cross section for the RP in millibarns with its  $1\sigma$  uncertainty for the reaction  ${}^6\text{Li} + {}^{27}\text{Al}$  as a function of the excitation energy of the compound nucleus  ${}^{33}\text{S}$  in MeV using  $\sigma(\text{CF})$  from Ref. [21].

$E_{\text{CN}}$ (MeV)	${}^{25}\text{Mg}$	${}^{28}\text{Al}$	${}^{28}\text{Si}$	${}^{30}\text{P}$	${}^{31}\text{P}$	CF
27.9	$1.31 \pm 0.21$	$1.54 \pm 0.28$	$3.30 \pm 0.78$	$0.32 \pm 0.06$	$0.58 \pm 0.18$	$1.88 \pm 0.59$
28.7	$5.6 \pm 0.8$	$7.6 \pm 1.0$	$15.8 \pm 3.8$	$1.24 \pm 0.25$	$4.3 \pm 0.9$	$13.6 \pm 3.6$
29.6	$16.1 \pm 2.4$	$21 \pm 3$	$42 \pm 10$	$1.37 \pm 0.28$	$20 \pm 3$	$52.1 \pm 8.8$
30.4	$37 \pm 5$	$55 \pm 7$	$105 \pm 25$	$6.7 \pm 1.4$	$50 \pm 8$	$128 \pm 22$
31.2	$56 \pm 8$	$84 \pm 10$	$123 \pm 30$	$7.5 \pm 1.5$	$69 \pm 12$	$216 \pm 36$
32.0	$61 \pm 9$	$66 \pm 8$	$124 \pm 30$	$13.6 \pm 2.7$	$94 \pm 16$	$291 \pm 49$
32.8	$83 \pm 13$	$78 \pm 10$	$136 \pm 33$	$14.6 \pm 2.9$	$110 \pm 19$	$393 \pm 66$
33.6		$93 \pm 11$	$144 \pm 35$	$20 \pm 4$	$124 \pm 21$	

spectra after the end of the irradiation and the decay of the RP the nuclides  ${}^{28}\text{Al}$  and  ${}^{30}\text{P}$  (511-keV annihilation peak) were determined. The applied branching ratios are those used in Ref. [21] for the reaction  ${}^{17}\text{O} + {}^{16}\text{O}$ .

As already mentioned, the excitation functions for the RP were derived from the ratios  $\sigma(\text{RP})/\sigma({}^{31}\text{P})$  under the assumption that  ${}^{31}\text{P}$  is produced only via the compound nucleus  ${}^{33}\text{S}$ . The ratio  $\sigma({}^{31}\text{P})/\sigma(\text{CF})$  is taken from Thomas *et al.* [21]. If any of the used partial cross sections include a contribution of a reaction which omits the way via the compound nucleus then  $\sigma(\text{CF})$  becomes too large. Several calculations were performed to test if the shape of  $\sigma(\text{CF})$  complies with the predictions of the compound nucleus model. Calculations by EMPIRE [22] give generally larger ratios than derived from Ref. [21] (Fig. 10). Further calculations (CCFULL [28] and NRV [34]) can explain this because these calculations give smaller  $\sigma(\text{CF})$  below the CB than those given in Ref. [21].

From the  ${}^6\text{Li} + {}^{27}\text{Al}$  experiments the cross sections for the formation of  ${}^{28}\text{Si}$ ,  ${}^{25}\text{Mg}$ , and  ${}^{28}\text{Al}$  could be determined. Interestingly, the ratios  $\sigma({}^{28}\text{Si})/\sigma(\text{CF})$  and  $\sigma({}^{25}\text{Mg})/\sigma(\text{CF})$  significantly increase below the CB compared with the ratios derived from the reaction  ${}^{17}\text{O} + {}^{16}\text{O}$  (Figs. 11 and 12).

Similar calculations as for the reaction  ${}^7\text{Li} + {}^{27}\text{Al}$  were performed but the significant increase in the ratios  $\sigma(\text{RP})/\sigma(\text{CF})$  at lower energies could not be reproduced by pure statistical model reaction codes.

#### IV. CONCLUSION

Cross sections for the formation of several RPs derived from measured  $\gamma$ -ray production cross sections for transitions in these nuclei or their decay products from the nuclear

reaction  ${}^7\text{Li} + {}^{27}\text{Al}$  showed significant differences compared with reaction  ${}^{18}\text{O} + {}^{16}\text{O}$ . Both reactions are producing the compound nucleus  ${}^{34}\text{S}$ . However, below the CB the ratios  $\sigma(\text{RP})/\sigma(\text{CF})$  increased substantially for the weakly bound projectile  ${}^7\text{Li}$  whereas for the tightly bound reaction partners  ${}^{18}\text{O}$  and  ${}^{16}\text{O}$  the ratio remains rather constant. The same effect could be observed when comparing the reaction  ${}^6\text{Li} + {}^{27}\text{Al}$  with the reaction  ${}^{17}\text{O} + {}^{16}\text{O}$ . We conclude a strong contribution of a direct reaction process, such as a breakup reaction and/or transfer reaction in case of the weakly bound projectile whereas the ratios  $\sigma(\text{RP})/\sigma(\text{CF})$  remain rather constant for a pure compound nucleus reaction.

Calculations by EMPIRE [22] reproduce the cross sections for the reaction  ${}^{18}\text{O} + {}^{16}\text{O}$  sufficiently well, even below the CB [e.g., see Figs. 9(a) and 9(b), 11, and 12]. However, the increased production rates for the RP below the CB could not be reproduced for the reaction  ${}^7\text{Li} + {}^{27}\text{Al}$  as well as for  ${}^6\text{Li} + {}^{27}\text{Al}$  which clearly hint for another reaction mechanism. Coupled-channel calculation with the computer code CCFULL [28] and a calculation using a proximity potential [31–33] give results for  $\sigma(\text{CF})$  which fit much better to the measured data. We conclude that below the CB with decreasing energy the breakup and/or transfer reaction become the dominant reaction channels for weakly bound projectiles. A possible explanation may be the cluster structure of the light projectiles  ${}^6\text{Li}$  ( $\alpha + d$ ) and  ${}^7\text{Li}$  ( $\alpha + t$ ) compared with the magic oxygen isotopes.

Tables II and III summarize the cross sections and its  $1\sigma$  uncertainties derived from the measured cross-section ratios and the cross section for complete fusion taken from Ref. [21].

- [1] H. Geissel, G. Muenzenberg, and K. Riisager, Secondary Exotic Nuclear Beams, *Annu. Rev. Nucl. Part. Sci.* **45**, 163 (1995).
- [2] Vandana Tripathi, A. Navin, K. Mahata, K. Ramachandran, A. Chatterjee, and S. Kailas, Angular Momentum and Cross Sections for Fusion with Weakly Bound Nuclei: Breakup, a Coherent Effect, *Phys. Rev. Lett.* **88**, 172701 (2002).
- [3] M. Dasgupta, P. R. S. Gomes, D. J. Hinde, S. B. Moraes, R. M. Anjos, A. C. Berriman, R. D. Butt, N. Carlin, J. Lubian, C. R. Morton, J. O. Newton, and A. Szanto de Toledo, Effect of breakup on the fusion of  ${}^6\text{Li}$ ,  ${}^7\text{Li}$ , and  ${}^9\text{Be}$  with heavy nuclei, *Phys. Rev. C* **70**, 024606 (2004).
- [4] J. M. Figueira, J. O. Fernández Niello, A. Arazi, O. A. Capurro, P. Carnelli, L. Fimiani, G. V. Martí, D. Martínez Heimann, A. E. Negri, A. J. Pacheco, J. Lubian, D. S. Monteiro, and P. R. S. Gomes, Energy dependence of the optical potential of weakly and tightly bound nuclei as projectiles on a medium-mass target, *Phys. Rev. C* **81**, 024613 (2010).
- [5] P. K. Rath, S. Santra, N. L. Singh, R. Tripathi, V. V. Parkar, B. K. Nayak, K. Mahata, R. Palit, Suresh Kumar, S. Mukherjee, S. Appannababu, and R. K. Choudhury, Suppression of complete fusion in the  ${}^6\text{Li} + {}^{144}\text{Sm}$  reaction, *Phys. Rev. C* **79**, 051601(R) (2009).

- [6] D. J. Hinde, M. Dasgupta, B. R. Fulton, C. R. Morton, R. J. Wooliscroft, A. C. Berriman, and K. Hagino, Fusion Suppression and Sub-Barrier Breakup of Weakly Bound Nuclei, *Phys. Rev. Lett.* **89**, 272701(2002).
- [7] V. V. Parkar, K. Mahata, S. Santra, S. Kailas, A. Shrivastava, K. Ramachandran, A. Chatterjee, V. Jha, and P. Singh, Fusion cross sections for  ${}^7\text{Li} + {}^{12}\text{C}$  system at near barrier energies, *Nucl. Phys. A* **792**, 187 (2007).
- [8] A. Mukherjee, U. Datta Pramanik, S. Chattopadhyay, M. Saha Sarkar, A. Goswami, P. Basu, R. Bhattacharya, M. L. Chatterjee, and B. Dasmahapatra, Investigation of  ${}^6\text{Li} + {}^{16}\text{O}$  and  ${}^7\text{Li} + {}^{16}\text{O}$  reactions at low energies, *Nucl. Phys. A* **645**, 13 (1999).
- [9] A. Mukherjee, U. Datta Pramanik, S. Chattopadhyay, M. Saha Sarkar, A. Goswami, P. Basu, R. Bhattacharya, M. L. Chatterjee, and B. Dasmahapatra, Fusion cross sections for  ${}^6\text{Li} + {}^{12}\text{C}$  and  ${}^6\text{Li} + {}^{13}\text{C}$  reactions at low energies, *Nucl. Phys. A* **635**, 305 (1998).
- [10] A. Mukherjee, M. Dasgupta, D. J. Hinde, H. Timmers, R. D. Butt, and P. R. S. Gomes, Absence of fusion suppression due to breakup in the  ${}^{12}\text{C} + {}^7\text{Li}$  reaction, *Phys. Lett. B* **526**, 295 (2002).
- [11] M. Ray, A. Mukherjee, M. K. Pradhan, Ritesh Kshetri, M. Saha Sarkar, R. Palit, I. Majumdar, P. K. Joshi, H. C. Jain, and B. Dasmahapatra, Fusion cross sections for  ${}^6,7\text{Li} + {}^{24}\text{Mg}$  reactions at energies below and above the barrier, *Phys. Rev. C* **78**, 064617 (2008).
- [12] A. Pakou, N. Alamanos, G. Doukelis, A. Gillibert, G. Kalyva, M. Kokkoris, S. Kossionides, A. Lagoyannis, A. Musumarra, C. Papachristodoulou, N. Patronis, G. Perdikakis, D. Pierroutsakou, E. C. Pollacco, and K. Rusek, Elastic scattering of  ${}^7\text{Li} + {}^{28}\text{Si}$  at near-barrier energies, *Phys. Rev. C* **69**, 054602 (2004).
- [13] E. de Barbará, G. V. Martí, A. Arazi, O. A. Capurro, J. O. Fernández Niello, J. M. Figueira, A. J. Pacheco, M. Ramírez, M. D. Rodríguez, J. E. Testoni, M. Verruno, I. Padrón, P. R. S. Gomes, and E. Crema, Fusion cross sections for the  ${}^6,7\text{Li} + {}^{27}\text{Al}$ ,  ${}^9\text{Be} + {}^{27}\text{Al}$  systems, in *VI Latin American Symposium on Nuclear Physics and Applications*, edited by A. J. Kreiner, O. Civitarese, C. Dorso, G. G. Bermudez, A. J. Pacheco, and N. N. Scozzola, AIP Conf. Proc. No. 884 (AIP, New York, 2007), p. 189.
- [14] L. R. Gasques, J. Hinde, M. Dasgupta, A. Mukherjee, and R. G. Thomas, Suppression of complete fusion due to breakup in the reactions  ${}^{10,11}\text{B} + {}^{209}\text{Bi}$ , *Phys. Rev. C* **79**, 034605 (2009).
- [15] W. Loveland, A. M. Vinodkumar, R. S. Naik, P. H. Sprunger, B. Matteson, J. Neeway, M. Trinczek, M. Domsbky, P. Machule, D. Ottewell, D. Cross, K. Gagnon, and W. J. Mills, Sub-barrier fusion of  ${}^9\text{Li}$  with  ${}^{70}\text{Zn}$ , *Phys. Rev. C* **74**, 064609 (2006).
- [16] S. Hudan, R. T. deSouza, A. S. Umar, Z. Lin, and C. J. Horowitz, Enhanced dynamics in fusion of neutron-rich oxygen nuclei at above-barrier energies, *Phys. Rev. C* **101**, 061601(R) (2020).
- [17] Varinderjit Singh, J. Vadas, T. K. Steinbach, B. B. Wiggins, S. Hudan, R. T. deSouza, Zidu Lin, C. J. Horowitz, L. T. Baby, S. A. Kuvin, Vandana Tripathi, I. Wiedenhöver, and A. S. Umar, Fusion enhancement at near and sub-barrier energies in  ${}^{19}\text{O} + {}^{12}\text{C}$ , *Phys. Lett. B* **765**, 99 (2017).
- [18] Y. Eyal, M. Beckerman, R. Chechik, Z. Fraenkel, and H. Stocker, Nuclear size and boundary effects on the fusion barrier of oxygen with carbon, *Phys. Rev. C* **13**, 1527 (1976).
- [19] R. T. deSouza, Varinderjit Singh, S. Hudan, Z. Lin, and C. J. Horowitz, Effect of increasing neutron-excess on the fusion cross-section in  ${}^{12-15}\text{C} + {}^{12}\text{C}$  at above-barrier energies, *Phys. Lett. B* **814**, 136115 (2021).
- [20] L. F. Canto, P. R. S. Gomes, R. Donangelo, and M. S. Hussein, Fusion and breakup of weakly bound nuclei, *Phys. Rep.* **424**, 1 (2006).
- [21] J. Thomas, Y. T. Chen, S. Hinds, D. Meredith, and M. Olson, Sub-barrier fusion of the oxygen isotopes: A more complete picture, *Phys. Rev. C* **33**, 1679 (1986).
- [22] M. Herman, R. Capote, B. V. Carlson, P. Obložinský, M. Sin, A. Trkov, H. Wienke, and V. Zerkin, EMPIRE: Nuclear Reaction Model Code System for Data Evaluation, *Nucl. Data Sheets* **108**, 2655 (2007).
- [23] W. Kutschera, P. Collon, H. Friedmann, R. Golser, P. Hille, A. Priller, W. Rom, P. Steier, S. Tagesen, A. Wallner, E. Wild, and G. Winkler, VERA: A new AMS facility in Vienna, *Nucl. Instrum. Methods Phys. Res., Sect. B* **123**, 47 (1997).
- [24] O. Forstner, P. Törnström, H. Friedmann, P. Hille, J. Kühtreiber, A. Pavlik, and A. Priller, Light ion induced nuclear reactions close to the Coulomb barrier, *J. Phys.: Conf. Series* **312**, 082021 (2011).
- [25] J. F. Ziegler and J. P. Biersack, SRIM-2003-the stopping and range of ions in matter, Program package, <http://www.srim.org/>.
- [26] NNDC, Brookhaven National Laboratory, NUDAT 2.7, <http://www.nndc.bnl.gov/nudat2/>.
- [27] T. Watanabe, Y. Oi, M. Taki, K. Kawasaki, and M. Yoshida, Evaluation of peak-to-total ratio for germanium detectors, *Appl. Radiat. Isot.* **50**, 1057 (1999).
- [28] K. Hagino, N. Rowley, and A. T. Kruppa, A program for coupled-channel calculations with all order couplings for heavy-ion fusion reactions, *Comput. Phys. Commun.* **123**, 143 (1999).
- [29] K. Kalita, S. Verma, R. Singh, J. J. Das, A. Jhingan, N. Madhavan, S. Nath, T. Varughese, P. Sugathan, V. V. Parkar, K. Mahata, K. Ramachandran, A. Shrivastava, A. Chatterjee, S. Kailas, S. Barua, P. Basu, H. Majumdar, M. Sinha, R. Bhattacharya, and A. K. Sinha, Elastic scattering and fusion cross sections for  ${}^7\text{Be}$ ,  ${}^7\text{Li} + {}^{27}\text{Al}$  systems, *Phys. Rev. C* **73**, 024609 (2006).
- [30] I. Padron, P. R. S. Gomes, R. M. Anjos, J. Lubian, C. Muri, J. J. S. Alves, G. V. Marti, M. Ramirez, A. J. Pacheco, O. A. Capurro, J. O. Fernández Niello, J. E. Testoni, D. Abriola, and M. R. Spinella, Fusion of stable weakly bound nuclei with  ${}^{27}\text{Al}$  and  ${}^{64}\text{Zn}$ , *Phys. Rev. C* **66**, 044608 (2002).
- [31] I. Dutt, The role of various parameters used in proximity potential in heavy-ion fusion reactions: New extension, *Pramana* **76**, 921 (2011).
- [32] W. D. Myers and W. J. Świątecki, Nucleus-nucleus proximity potential and superheavy nuclei, *Phys. Rev. C* **62**, 044610 (2000).
- [33] K. Siwek-Wilczyńska and J. Wilczyński, Empirical nucleus-nucleus potential deduced from fusion excitation functions, *Phys. Rev. C* **69**, 024611 (2004).
- [34] V. Zagrebaev *et al.*, Nuclear Reactions Video Project (Knowledge Base on Low Energy Nuclear Physics), <http://nrv.jinr.ru/nrv/>.